PHYSICAL REVIEW B **71**, 205416 (2005)

In situ assessment of carbon nanotube diameter distribution with photoelectron spectroscopy

T. de los Arcos,[1,*] M. G. Garnier,[1,†] P. Oelhafen,[1] J. W. Seo,[2] C. Domingo,[3] J. V. García-Ramos,[3] and S. Sánchez-Cortés[3]
[1]*Institute of Physics, University of Basel, Klingelbergstrasse 82, 4056 Basel, Switzerland*
[2]*Institute of Physics of Complex Matter, EPFL, Ecublens, CH-1015 Lausanne, Switzerland*
[3]*Instituto de Estructura de la Materia, CSIC, c/Serrano 123, 28006 Madrid, Spain*
(Received 17 December 2004; published 27 May 2005)

In situ UV-photoelectron spectroscopy (He I and He II) was performed on multiwalled carbon nanotubes (CNTs) with clearly differentiated diameter distributions. A significant dependence of valence- and conduction-band characteristics on the mean CNT diameter was observed, which was determined by high-resolution TEM and micro-Raman spectroscopy. The decrease of relative intensity of the π states at −3 eV in the He II experiments, indicative of increasing rehybridization between orbitals, was directly correlated with decreasing mean diameters. Furthermore, a progressive broadening of the unoccupied σ^* band at 7.6 eV was found in the He I spectra.

DOI: 10.1103/PhysRevB.71.205416 PACS number(s): 73.22.−f, 79.60.Jv, 61.46.+w

I. INTRODUCTION

Photoelectron spectroscopy (PES) is a macroscopic technique that can be used to directly measure electronic states. In particular, UV-photoelectron spectroscopy (UPS) has proven to be an extremely useful tool in the determination of the valence-band electronic structure of carbon-based materials,[1–3] including carbon nanotubes (CNTs).[4–8] However, UPS measurements usually require samples of macroscopic dimensions. In particular, for the clarification of fundamental electronic properties by UPS, monodispersed CNT samples would be required, which at present is no trivial task. The typical chemical vapor deposition (CVD) processes commonly result in broad CNT distributions (broader than those obtained by arc discharge or laser ablation), even though substantial narrowing of nanotube-diameter distributions has been achieved by different approaches: for example, by using preformed catalyst particles with narrow-diameter distributions (see Refs. 9 and 10 and references therein), using porous supports such as silica or alumina,[11,12] or applying fullerenes as carbon stock.[13] Hence, typical CNT samples consist of a more or less wide mixture of diameters and result in a mixture of different electronic characteristics. With the exception of the recent work of Ishii *et al.* on purified, single-walled nanotubes (SWNTs),[14] UPS studies have been systematically performed on nonmonodispersed samples, so that the measured electronic structure represents an average of different contributions. Consequently, the effect of curvature on the electronic characteristics of CNTs has not been directly accessible by UPS. Most of the experimental investigations related to the correlation between the CNT curvature and the electronic structures have been realized with other techniques, such as electron-energy-loss spectroscopy (EELS)[15–17] or x-ray absorption,[18] which allow measurements on individual nanotubes.

In this paper, samples of multiwalled CNTs with different diameter distributions were investigated. They were grown by a CVD technique onto Si substrates, either bare or covered with buffer layers of Al_2O_3, TiN, or TiO_2. As we have shown previously, the different buffer layers yielded clearly differentiated CNT-diameter distributions, due to chemical and morphological interaction between the catalyst and the buffer layer.[19,20] In the present paper, we show *in situ* UPS measurements and correlate the spectral features with the CNT diameter determined by conventional *ex situ* characterization methods, high-resolution TEM, and micro-Raman spectroscopy. We illustrate that the UPS spectral features in the valence and conduction bands are directly correlated with the CNT curvature and therefore can be used as markers to estimate the upper and lower limits of the CNT-diameter distributions. Moreover, we report on the broadening of the unoccupied σ^* band at −7.6 eV in the He I spectra, which clearly shows a CNT-diameter dependence. To the best of our knowledge this feature has not been reported until now, and it provides additional details about the electronic structure of CNTs. Our results demonstrate how UPS can be applied as an additional, important characterization technique beside high-resolution TEM and Raman spectroscopy.

II. EXPERIMENTAL SETUP

The experimental setup consisted of a high-vacuum chamber (background pressure 10^{-6} mbar) adapted for carbon-nanotube growth, attached to an ultrahigh-vacuum (UHV) chamber housing a photoelectron spectrometer (Leybold EA10N). The nanotubes described in this work were grown directly onto Si wafers (100) or onto Si wafers covered with thin (20–80 nm) buffer layers of Al_2O_3, TiN, or TiO_2, using sputtered Fe as a catalyst. The Si substrates were rinsed consecutively in acetone and ethanol in an ultrasonic bath prior to introduction in the vacuum chamber, and no further *in situ* cleaning procedures were performed. Therefore, all Si substrates used were covered with their native SiO_2 layers, with an estimated thickness of 2 nm. The samples were first annealed in a vacuum up to 840 °C and then exposed to acetylene during 5 min, at a gas pressure of 0.1 mbar and 55 sccm flow. All process steps (deposition of buffer layer and catalyst, annealing, and acetylene exposure) were performed sequentially inside the chamber, without exposure to air. (For a detailed description of sample preparation and buffer-layer characteristics see Refs. 19 and 20.)

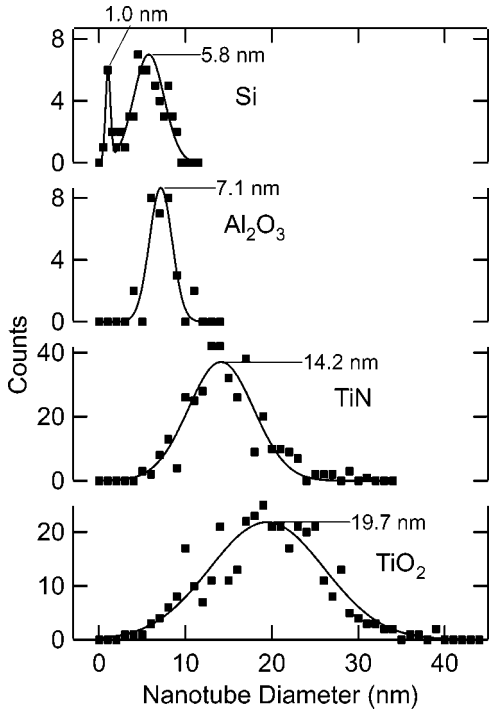

FIG. 1. Diameter distribution as determined from high-resolution TEM analysis of carbon nanotubes grown onto different buffer layers under identical experimental conditions. The measured values are fitted with Gaussian functions.

After CVD, the samples were allowed to cool and were transferred to the UHV chamber for x-ray photoelectron spectroscopy (XPS) and UPS analysis without breaking the vacuum. The samples were always measured directly after growth, and they did not undergo any kind of cleaning procedure. For XPS, Mg Kα excitation was employed, with a spectral resolution of 0.9 eV. The energy position of each spectrum was calibrated with reference to the $4f_{7/2}$ level of a clean gold sample, at 84.0 eV binding energy. For the UPS analysis, a He lamp was used with 21.2 eV (He I) and 40.8 eV (He II) excitation energies. The Fermi level of a clean Au sample was used as a reference.

After a first *in situ* characterization with PES, the samples were further analyzed *ex situ* by high-resolution transmission electron microscopy (TEM, Philips CM20 and CM300) and micro-Raman spectroscopy. The Raman spectrometer was a Renishaw RM1000 with laser excitation at 785 nm (1.58 eV) and a 2-μm laser spot.

III. EXPERIMENTAL RESULTS AND DISCUSSION

We present in the first place the analysis of the CNT structure based on well-established *ex situ* characterization techniques in order to facilitate the forthcoming discussion about PES-data interpretation.

A. Ex situ: TEM and Raman measurements

In Fig. 1 we present nanotube-diameter distributions extracted from the TEM analysis of CNTs grown onto different substrates: Si substrates covered with the native oxide layer and with additional coverage of buffer layers of Al_2O_3, TiN, or TiO_2. Typical high resolution TEM images of these samples are additionally presented in Fig. 2. The different interaction and chemical transformations of Fe onto the different underlying substrate materials lead to CNTs with distinctive diameter ranges even though all samples were grown under identical experimental conditions of temperature and gas pressure.[19,20] As we can see in Fig. 1, CNT mean diameters range from 20 nm onto TiO_2 (with more than 30 walls) to 6 nm onto Si and Al_2O_3 (2–5 walls). The thinnest CNTs were found among the samples grown directly onto bare Si, as we can see in the second distribution peak at 1.0 nm. However, in this case the obtained CNT density was low because of the FeSi formation, which reduced the catalytic efficiency of Fe.[21]

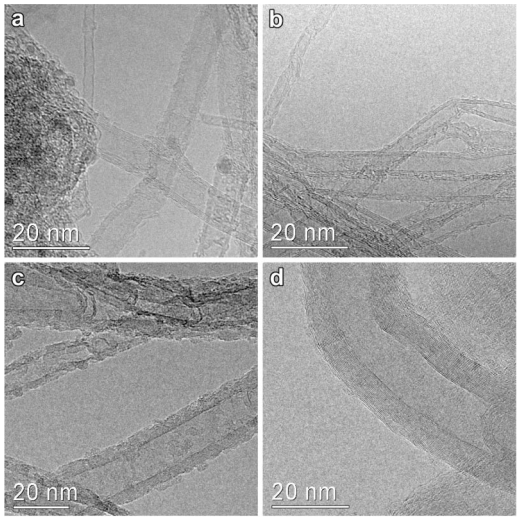

FIG. 2. Typical high-resolution TEM images of carbon nanotubes grown (a) directly onto Si or onto different buffer layers of (b) Al_2O_3, (c) TiN, (d) TiO_2.

In Fig. 3 we can see the Raman spectra corresponding to the same CNT samples, compared with polycrystalline graphite and highly oriented pyrolytic graphite (HOPG) samples. In the region between 1100–1800 cm^{-1} we have the signals corresponding to the *D*, *G*, and *D'* bands. The *D* and *D'* bands at $\sim$1315 cm^{-1} and 1614 cm^{-1}, respectively, were activated in general by any structural change that broke the symmetry of the planar graphene sheets, such as the presence of small graphite crystals. The *G* band, at $\sim$1584 cm^{-1}, was due to in-plane stretching of the C atoms in the graphene layers. From the intensity ratio between the *D* and *G* bands, it is possible to estimate the degree of perfection of the graphene planes in the graphite samples.[22,23] Thus, according to the work of Tuinstra and Koenig[23] we find a mean crystallite size of the order of 3 nm in our polycrystalline graphite sample and one of $\sim$1 μm in HOPG. In principle we could also use this intensity ratio in the case of CNTs to determine the degree of crystallinity of the walls. However, a recent Raman analysis of multiwalled nanotubes (MWNTs) suggests that both *D* and *D'* bands are intrinsic features of the Raman spectrum of MWNTs, and they are not necessarily an indication of a disordered wall structure.[24] Therefore,

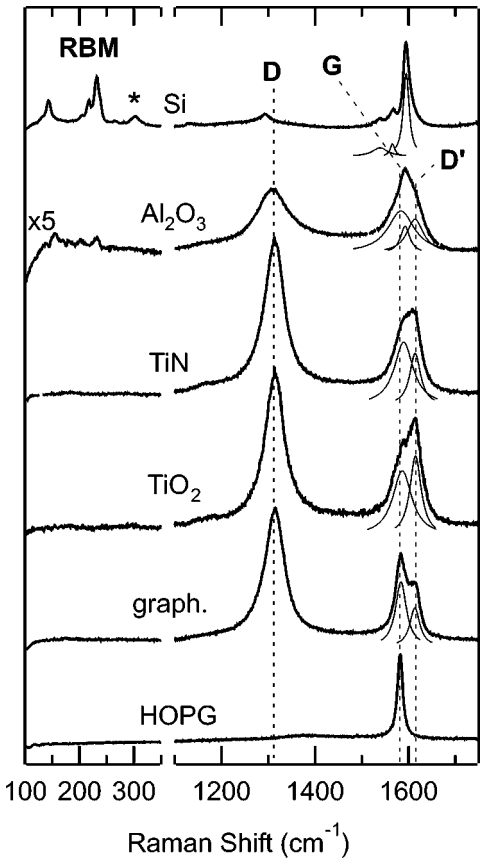

FIG. 3. Raman spectra (λ_{laser}=785 nm) of CNT samples grown onto Si substrates covered with different buffer layers, compared to the spectra of HOPG and polycrystalline graphite. The spectra have been normalized to the intensity of the *G* band. The band marked with an asterisk corresponds to the Si substrate.

the Tuinstra-Koenig relationship should not be applied to quantitatively determine the size of perfectly graphitized domains onto the CNT walls. Nevertheless, the high intensity of the *D* bands in the TiO_2- and TiN-grown CNTs reflects the twisted structures observed with TEM and scanning electron microscopy (SEM) (not shown here), as compared with the relatively straight tubes grown onto Al_2O_3, or Si.[19,20] Following a Lorentzian line-shape analysis of the spectra, we recognize in the CNTs grown onto TiO_2 or TiN the same features as in polycrystalline graphite, with *D*, *G*, and *D'* bands at approximately 1315 cm^{-1}, 1585 cm^{-1}, and 1614 cm^{-1}. In the case of the thinner CNTs grown onto Al_2O_3, we have an intermediate case. In the *G* band we find the graphitelike features at 1585 and 1614 cm^{-1}, originating from the outer walls of the tubes, together with a weak resonant contribution at 1592 cm^{-1} from the tubes in a diameter range around 1–2 nm.[25] Since no tubes with this outer diameter were found in the TEM analysis, we attribute this resonant contribution to some of the inner tubes in the appropriate diameter range. (The number of walls in these CNTs oscillates between 2 and 5, approximately.) The resonance is additionally seen in the region under ~300 cm^{-1}, where the bands associated to the radial breathing modes (RBMs) are present. The RBMs correspond to the collective in-phase radial vibrations of the CNTs that are not present in other types of graphitic materials. They are extremely diameter dependent and are only visible when the frequency of the transition and the laser wavelength are in resonance.[26] In the case of the CNTs grown onto Si, the intense resonant contribution of the nanotubes with ~1.0 nm diameter masks the weaker nonresonant contributions to the Raman spectrum coming from thicker tubes in the 6-nm-diameter range. We see intense RBMs, corresponding to single- or double-walled nanotubes, together with a characteristic splitting of the *G* band at 1539, 1566, and 1594 cm^{-1} and a profile corresponding to semiconducting tubes.

B. In situ: PES measurements

As already mentioned in the description of the experimental setup, CNT samples were transferred to the PES measurement chamber immediately after growth, without breaking the vacuum. Firstly, the chemical composition of the samples was determined by XPS analysis (not shown here). This analysis showed that the samples were only composed of carbon. No traces of the original iron catalyst or oxygen contamination were found (the detection limits for Fe and O under our measurement conditions were 0.2 and 1.3 at. %, respectively). The only exception was the sample grown directly onto Si, but the measured concentrations of oxygen, silicon, and iron (8, 7, and 2 at. % respectively) correspond to that of the substrate, which contribute to the measurement due to the low CNT coverage.[21]

After the first XPS analysis, the samples were investigated with UV photons emitted from a He lamp at mostly two different energies: 40.8 eV (He II) and 21.2 eV (He I). Since the mean-free path of electrons depends on their kinetic energies,[27] we sampled the CNTs at different depths. Taking an average interwall distance of 0.335 nm, we can estimate the information depth for the different photons as being one–two walls with He II, three walls with He I, and about six walls with XPS (1253.6 eV).

1. He II (hν=40.8 eV)

In Fig. 4, the spectra of the CNT samples and polycrystalline graphite, measured with 40.8 eV of photon energy (He II), are shown. The most prominent features are at −7.8 eV, assigned mostly to σ states (sp^2 orbitals), and at around −3 eV, assigned to π states (p_z orbitals).[28–31] In the upper part of the figure, spectra have been superimposed after the subtraction of a Shirley background and normalization to the −7.8 eV band for a better comparison. As already reported by Chen and co-workers[4,32] the intensity of the π states at −3 eV is always lower for CNTs than for graphite, due to the rehybridization of π orbitals arising from the curved nature of the CNT walls.[33–35] The rehybridization lowers the relative intensity of π states by a factor dependent on the curvature. (Ajayan *et al.*[15] also observed with EELS a gradual decrease of the intensity of the π-electron plasmon with a decreasing diameter.) In our case, even though the measured intensity of π states corresponds to the average value of CNTs within a broad diameter range, there is a clear difference in intensity between samples grown on TiN or TiO_2 buffer layers, with nanotube diameters up to

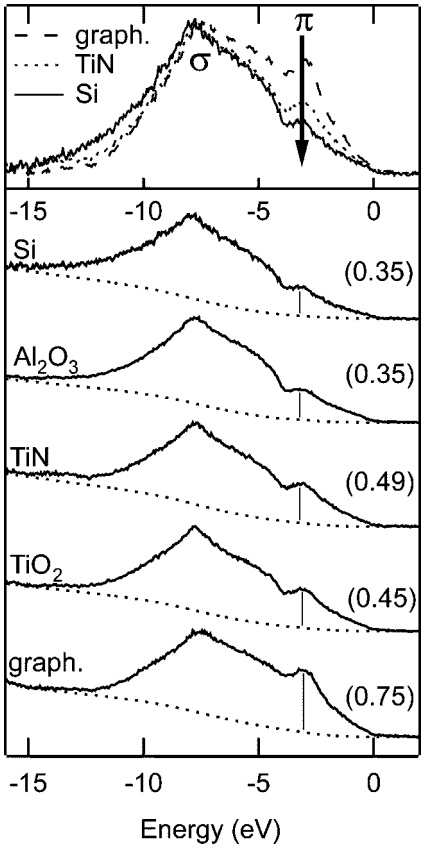

FIG. 4. He II (40.8 eV) spectra of CNT samples grown onto Si substrates covered with different buffer layers and spectra of polycrystalline graphite. The spectra are normalized to the band at −7.8 eV. The numbers in parentheses correspond to the intensity of the π states at −3 eV after background substraction. In the upper part, the spectra corresponding to graphite and to nanotubes grown onto TiN and Si are superposed after removal of the Shirley background, for a better comparison.

20–30 nm, and the Al_2O_3 and Si, with a maximum diameter up to 10 nm and narrower distributions.

2. He I (hν=21.2 eV)

Figure 5 shows the spectra measured with He I radiation. The most pronounced difference between the He II and He I measurements is the appearance of intense bands in the energy range below −10 eV in the latter ones. These new features correspond to photoelectrons that, after being scattered into the flat conduction bands of graphite, arrive to the detector at fixed kinetic-energy values. The dependence of the position of these spectral features with photon energy makes it possible to discriminate between occupied states (at fixed binding-energy values) and unoccupied states (at fixed kinetic-energy values, whose apparent binding energy depends on the photon energy used). In any case, the He I spectra are dominated by an intense band centered at −13.6 eV that shows a clear broadening with diminishing CNT-mean diameter. Unfortunately, the high background of inelastically scattered electrons makes, in this case, a quantitative comparison of the spectra difficult, especially since the bands of interest lie in the lower kinetic-energy range, close to the spectrometer cutoff.

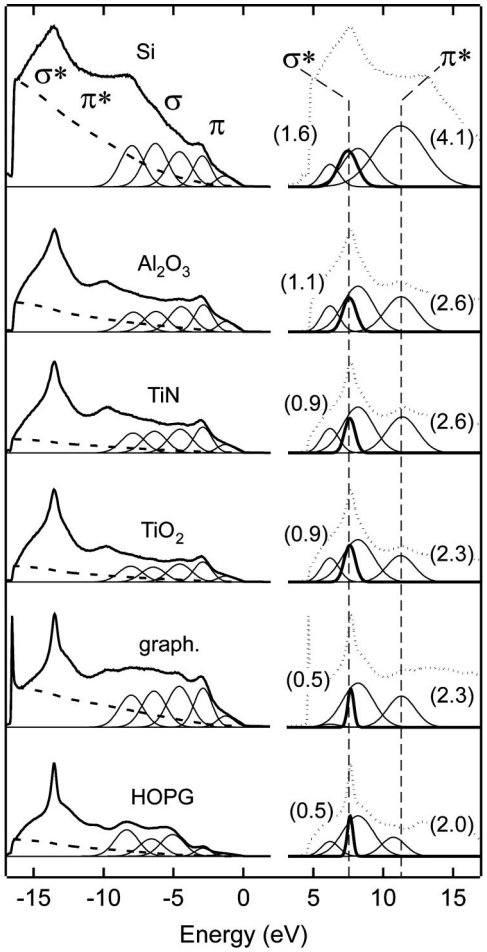

FIG. 5. He I (21.2 eV) spectra of CNT samples grown onto Si substrates covered with different buffer layers, polycrystalline graphite, and HOPG. The original spectra are represented on the negative side of the energy scale, together with the corresponding Shirley backgrounds (dashed lines). The spectra were decomposed into nine Gaussian components, four of which are associated with unoccupied states, in the positive side of the energy scale. The dotted lines represent the original spectra, displaced to the positive-energy side. The numbers in parentheses correspond to the widths of the Gaussian curves used to fit the σ^* and π^* bands at 7.6 eV and 11 eV, respectively. For more information about the decomposition and assignment of the Gaussian components, see Table I.

In order to enable a quantitative comparison, each spectrum was decomposed into nine Gaussian components after the subtraction of a Shirley background and normalization to the narrow band at −13.6 eV. We want to emphasize that the main reason behind this decomposition was to obtain an estimated comparison between samples. Therefore, although the Gaussian components have been assigned to specific bands (see Table I), this purely mathematical decomposition is not a representation of the electronic density of states. With respect to the work of Takahashi *et al.*[36] we assigned the four Gaussian components with energies under −10 eV to conduction states, whose real energy values are given by adding the photon energy to the apparent energy value. Accordingly, in Fig. 5 these components are presented in an absolute scale, in the positive-energy part of the spectrum.

TABLE I. Assignment and numerical values of the nine Gaussian components used in the decomposition of the He I spectra of CNTs and graphite. The diameter dependence of the π^* and σ^* bands are represented in Fig. 5. See text for details.

Assign.	E_B (eV) ±0.1	Width (eV)
π	−1.3	1.4±0.03
π	−2.9	1.5 (fixed)
σ	−4.5	2 (fixed)
σ	−6.4	2 (fixed)
σ	−8.0	2 (fixed)
π^*	11.3	diam. dependent
σ^*	8.2 (fixed)	2.6 (fixed)
σ^*	7.6	diam. dependent
Artifact	6.2 (fixed)	1.5 (fixed)

The bands at 7.6 and 8.2 eV correspond to σ^* states, while the broad band around 11 eV is assumed to be a mixture of σ^*, π^*, and valence-band states not properly decomposed by our mathematical treatment.

As can be seen in Table I, Gaussian curves associated with valence-band states had fixed widths in order to minimize the number of free mathematical parameters to fit. Among the three components used for the description of the conduction states, only the bands at 7.6 eV and ~11 eV were kept variable during the fit, in order to focus the comparative changes between spectra on these two components. This approach has to be modified once a better theoretical description of the band structure of MWNTs is available. Finally, the Gaussian component at 6.2 eV accounts mostly for the background electrons not described by the Shirley background near the spectrometer cutoff. Its position and width were also fixed.

In the following, we want to focus the discussion on the behavior of the narrow σ^* band at 7.6 eV. Although the band at ~11 eV also shows progressive width change for different samples, it is not clear in this case that the broadening is due only to changes in the CNT diameter. Since we have forced the nearby bands to have a fixed-width value, eventual changes in valence states not necessarily correlated to CNTs (such as, for example, an oxygen signal from the substrate for the Si sample) can be reflected in this band. On the other hand, the σ^* band at 7.6 eV is sufficiently separated from the rest of the valence-band features to ensure that we are only considering conduction states associated to CNTs.

Surprisingly, until now, this band has not attracted much interest in UPS studies of CNTs, possibly due to the high electronic background in the proximity of the spectrometer cutoff, which shows marked differences in the response for different spectrometers in this energy range. However, a clearly curvature-related broadening of this band with respect to the value of graphite was present in all of the CNT samples analyzed. The broadening of the band is not orientation related, since the polycrystalline graphite, where the whole range of different orientations is probed, shows the same bandwidth as the HOPG sample (~0.5 eV). Furthermore, the broadening is inversely correlated to the CNT diameter. This effect can be clearly seen in Fig. 6, where we gradually move from the full width half maximum (FWHM) values of 0.9 eV in the thicker CNTs grown onto TiN and TiO_2 to values of 1.6 eV in the case of the thinner tubes grown onto Si. Although FWHM values cannot be taken quantitatively due to the nonphysical band decomposition applied, it is clear that in comparative studies of different CNT samples the width of the σ^* band can provide valuable qualitative information related to the lower range of CNT-diameter distribution.

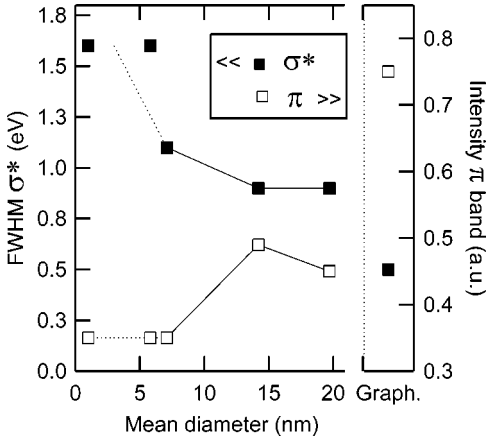

FIG. 6. Plot summarizing the observed effects as functions of mean nanotube diameter. The full symbols represent the FWHM of the σ^* band, obtained from the He I measurements. The hollow symbols represent the relative intensity of the π band in the He II spectra. The corresponding values for polycrystalline graphite are shown in the right-hand side of the figure. In order to emphasize the double-peaked diameter distribution observed in the CNTs grown directly onto Si (see Fig. 1), we have plotted the two values separately.

This band has been a strongly debated subject in the literature because of its interpretation as the so-called interlayer band, a concept proposed by Posternak *et al.*[37] The origin of this disagreement has already been thoroughly discussed in several papers dedicated to the electronic structure of graphite.[38,39] Briefly, the discrepancy arises from the fact that the interlayer band can be placed in two different positions with respect to the Fermi level, both supported by experimental information and theoretical calculations. For example, measurements with inverse photoemission spectroscopy and the calculations of Holzwarth *et al.*[31] place the interlayer band at around 4–5 eV, while PES, or secondary-electron-emission spectroscopy, supported by the calculations of Tatar and Rabii[30] place it at 7.5 eV. Recent studies on the electronic structure of graphite tend to support the calculations of Holzwarth *et al.*, placing the interlayer state at around 4–5 eV above the Fermi level.[39] However, when measuring photoemission one has to be careful, since Holzwarth *et al.* also predicted a strong dispersion along the direction perpendicular to the graphite planes (Γ-*A*). With 21.2 eV photon energy we are probing the graphite Brillouin zone near the *A* point (for $\mathbf{k}_{\|}=0$), and since the predicted band bottom at the *A* point is higher than that at the Γ point by about 3 eV, the band we observe at 7.6 eV could be com-

patible with both theoretical predictions. In any case, in one of the few PES studies carried out on CNTs so far using He I radiation, Suzuki *et al.* interpret the 7.6 eV band as the interlayer state, after observing its near disappearance in the spectrum of pure SWNTs.[5] However, based on our observations, their results can also be reinterpreted, considering that the 7.6 eV band has been practically smeared out, due to the broadening induced by the small diameter (1.4 nm) of the SWNTs.

At this point, we have not yet gained a full understanding of band broadening with decreasing nanotube diameter, although it is likely that this is an indication for a progressive increase in dispersion of the flat graphite conduction bands. There are a number of theoretical calculations related to the effect of curvature on the electronic structure of CNTs, but they mostly concentrate on SWNTs of small diameters, where the effect of rehybridization is greater.[34,40,41] The theoretical background of the electronic structure of the MWNTs has not yet been much explored, except for calculations made on double-walled nanotubes.[42,43] Particularly in Ref. 42 we find a rare attempt to simulate the electronic structure of the MWNTs. In any case, it remains difficult to correlate the conclusions extracted from the SWNTs of small diameters to the apparent increase of band dispersion, as we have observed in the samples composed mostly of MWNTs.

IV. SUMMARY

We performed a combined UPS, TEM, and Raman analysis of different CVD-grown CNT samples with diameters ranging between ~1 to ~30 nm and found a perfect correlation between the information obtained from the three techniques. In particular, by combining the He I and He II measurements of CNT samples we have obtained *in situ* information about CNT-diameter distribution immediately after the growth. In the He II measurements, the relative intensity of the π band at −3 eV decreases progressively as the reduction in CNT diameter forces higher orbital rehybridization. Additionally, we have seen for the first time in the He I measurements that the width of the σ^* band at 7.6 eV is also diameter dependent, and it broadens for narrower nanotubes. These two effects are summarized in Fig. 6. There is, therefore, a clear correlation of CNT curvature with the characteristics of valence- and conduction-band states, which can be used as markers to estimate the upper and lower limits of the CNT-diameter distributions in inhomogeneous samples. We have proven that UPS can successfully be applied to CNTs in order to extract information about diameter distribution. Since this technique also provides firsthand information on the effect that experimental parameters have on the diameter distribution of different samples, it is an important alternative to *ex situ* Raman spectroscopy, in particular in order to speed up the process of finding the appropriate experimental conditions.

ACKNOWLEDGMENTS

J.W.S. is grateful to the Centre Interdisciplinaire de Microscopie Electronique (CIME) at the Ecole Polytechnique Fédérale de Lausanne (EPFL) for access to TEM and technical support. We also thank the National Centre of Competence in Research for Nanoscience (NCCR) and the Swiss National Foundation for financial support.

*Electronic address: t.arcos@unibas.ch
†Present address: Institute of Physics, University of Neuchâtel, rue Breguet 1, 2000 Neuchâtel, Switzerland.

[1] P. Reinke and P. Oelhafen, J. Appl. Phys. **81**, 2396 (1999).
[2] P. Reinke and P. Oelhafen, Phys. Rev. B **60**, 15772 (1999).
[3] P. Reinke and P. Oelhafen, J. Chem. Phys. **116**, 9850 (2002).
[4] P. Chen, X. Wu, X. Sun, J. Lin, W. Ji, and K. L. Tan, Phys. Rev. Lett. **82**, 2548 (1999).
[5] S. Suzuki, C. Bower, Y. Watanabe, and O. Zhou, Appl. Phys. Lett. **76**, 4007 (2000).
[6] S. Suzuki, Y. Watanabe, T. Kiyokura, K. G. Nath, T. Ogino, S. Heun, W. Zhu, C. Bower, and O. Zhou, Phys. Rev. B **63**, 245418 (2001).
[7] S. Suzuki, C. Bower, T. Kiyokura, K. G. Nath, Y. Watanabe, and O. Zhou, J. Electron Spectrosc. Relat. Phenom. **114**, 255 (2001).
[8] S. Suzuki, Y. Watanabe, T. Ogino, S. Heun, L. Gregoratti, A. Barinov, B. Kaulich, M. Kishikiva, W. Zhu, C. Bower, and O. Zhou, Phys. Rev. B **66**, 035414 (2002).
[9] H. Ago, K. Nakamura, S. Imamura, and M. Tsuji, Chem. Phys. Lett. **391**, 308 (2004).
[10] Q. Fu, S. Huang, and J. Liu, J. Phys. Chem. B **108**, 6124 (2004).
[11] L. Huang, S. J. Wind, and S. P. O'Brien, Nano Lett. **3**, 299 (2003).
[12] M. J. Kim, T. Y. Lee, J. H. Choi, J. B. Park, J. S. Lee, S. K. Kim, J. B. Yoo, and C. Y. Park, Diamond Relat. Mater. **12**, 870 (2003).
[13] S. Maruyama, Y. Miyauchi, T. Edamura, Y. Igarashi, S. Chiashi, and Y. Murakami, Chem. Phys. Lett. **375**, 553 (2003).
[14] H. Ishii, H. Kataura, H. Shiozawa, H. Yoshioka, H. Otsubo, Y. Takayama, T. Miyahara, S. Suzuki, Y. Achiba, M. Nakatake, T. Narimura, M. Higashiguchi, K. Shimada, H. Namatame, and M. Taniguchi, Nature (London) **426**, 540 (2003).
[15] P. M. Ajayan, S. Iijima, and T. Ichihashi, Phys. Rev. B **47**, 6859 (1993).
[16] R. Kuzuo, M. Terauchi, M. Tanaka, and Y. Saito, Jpn. J. Appl. Phys., Part 1 **33**, L1316 (1994).
[17] O. Stéphan, P. M. Ajayan, C. Colliex, F. Cyrot-Lackmann, and É. Sandré, Phys. Rev. B **53**, 13824 (1996).
[18] C. L. Yueh, J. C. Jan, J. W. Chiou, W. F. Pong, M. H. Tsai, Y. K. Chang, Y. Y. Chen, Y. F. Lee, P. K. Tseng, S. L. Wei, C. Y. Wen, L. C. Chen, and K. H. Chen, Appl. Phys. Lett. **79**, 3179 (2001).
[19] T. de los Arcos, M. G. Garnier, P. Oelhafen, D. Mathys, J. W. Seo, C. Domingo, J. V. García-Ramos, and S. Sánchez-Cortés, Carbon **42**, 187 (2004).
[20] T. de los Arcos, M. G. Garnier, J. W. Seo, P. Oelhafen, V. Thommen, and D. Mathys, J. Phys. Chem. B **108**, 7728 (2004).
[21] T. de los Arcos, F. Vonau, M. G. Garnier, V. Thommen, P. Oelhafen, M. Düggelin, D. Mathis, and R. Guggenheim, Appl.

Phys. Lett. **80**, 2383 (2002).
[22] J. Kastner, T. Pichler, H. Kuzmany, S. Curran, W. Blau, D. N. Weldon, M. Delamesiere, S. Draper, and H. Zandbergen, Chem. Phys. Lett. **221**, 53 (1994).
[23] F. Tuinstra and J. L. Koenig, J. Chem. Phys. **53**, 1126 (1970).
[24] A. M. Rao, A. Jorio, M. A. Pimenta, M. S. S. Dantas, R. Saito, G. Dresselhaus, and M. S. Dresselhaus, Phys. Rev. Lett. **84**, 1820 (2000).
[25] X. Zhao, Y. Ando, L. Qin, H. Kataura, Y. Maniwa, and R. Saito, Appl. Phys. Lett. **81**, 2550 (2002).
[26] A. M. Rao, E. Richter, S. Bandow, B. Chase, P. C. Eklund, K. A. Williams, S. Fang, K. R. Subbaswamy, M. Menon, A. Thess, R. E. Smalley, G. Dresselhaus, and M. S. Dresselhaus, Science **275**, 187 (1997).
[27] D. A. Shirley, in *Photoemission in Solids I*, edited by M. Cardonaand L. Ley, Topics in Applied Physics Vol. 26 (Springer-Verlag, Berlin, 1978).
[28] G. S. Painter and D. E. Ellis, Phys. Rev. B **1**, 4747 (1970).
[29] F. R. McFeely, S. P. Kowalczyk, L. Ley, R. G. Cavell, and R. A. Pollak, Phys. Rev. B **9**, 5268 (1974).
[30] R. C. Tatar and S. Rabii, Phys. Rev. B **25**, 4126 (1982).
[31] N. A. W. Holzwarth, S. G. Louie, and S. Rabii, Phys. Rev. B **26**, 5382 (1982).
[32] P. Chen, X. Wu, J. Lin, H. Li, and K. L. Tan, Carbon **38**, 139 (2000).
[33] A. Kleiner and S. Eggert, Phys. Rev. B **64**, 113402 (2001).
[34] X. Blasé, L. X. Benedict, E. L. Shirley, and S. G. Louie, Phys. Rev. Lett. **72**, 1878 (1994).
[35] S. Okada and A. Oshiyama, Phys. Rev. Lett. **91**, 216801 (2003).
[36] T. Takahashi, H. Tokailin, and T. Sagawa, Phys. Rev. B **32**, 8317 (1985).
[37] M. Posternak, A. Baldereschi, A. J. Freeman, E. Wimmer, and M. Weinert, Phys. Rev. Lett. **50**, 761 (1983).
[38] F. Maeda, T. Takahashi, H. Ohsawa, S. Suzuki, and H. Suematsu, Phys. Rev. B **37**, 4482 (1988).
[39] J. Lehmann, M. Merschdorf, A. Thon, S. Voll, and W. Pfeiffer, Phys. Rev. B **60**, 17037 (1999).
[40] J. C. Charlier and P. Lambin, Phys. Rev. B **57**, R15037 (1998).
[41] S. Reich, C. Thomsen, and P. Ordejón, Phys. Rev. B **65**, 155411 (2002).
[42] D. Östling, D. Tománek, and A. Rosén, Phys. Rev. B **55**, 13980 (1997).
[43] Y. Miyamoto, S. Saito, and D. Tománek, Phys. Rev. B **65**, 041402(R) (2001).